Journal of Statistical Physics, Vol. 74, Nos. 1/2, 1994

Interfacial Growth in Driven Ginzburg–Landau Models: Short and Long-Time Dynamics

J. L. Mozos[1] and A. Hernández-Machado[1]

Received April 5, 1993; final July 19, 1993

Interfacial growth in driven systems is studied from the initial stage to the long-time regime. Numerical integrations of a Ginzburg–Landau type equation with a new flux term introduced by an external field are presented. The interfacial instabilities are induced by the external field. From the numerical results, we obtain the dispersion relation for the initial growth. During the intermediate temporal regime, fingers of a characteristic triangular shape could grow. Depending on the boundary conditions, the final state corresponds to strips, multifinger states, or a one-finger state. The results for the initial growth are interpreted by means of surface-driven and Mullins–Sekerka instabilities. The shape of the one-finger state is explained in terms of the characteristic length introduced by the external field.

KEY WORDS: Nonequilibrium steady state; interfacial instabilities; driven diffusive systems; Ginzburg–Landau model; external field.

1. INTRODUCTION

The study of spatiotemporal patterns induced by nonequilibrium interfacial instabilities constitutes an interesting field of research.[1-5] Relevant progress has been made in the characterization and selection of steady-state solutions[1-4] and increasing interest has been focused on the dynamics of evolution to a final state.[5-10] Examples of experimental systems in which such instabilities appear are directional solidification of binary alloys,[1-3] viscous fingering in Hele-Shaw cells,[4] and flames.[3] In a typical situation an interface separating two different phases, with an initial flat or circular

[1] Departament E.C.M., Facultat de Física, Universitat de Barcelona, E-08028 Barcelona, Spain. E-mail: AURORA@EBUBECM1.BITNET

0022-4715/94/0100-0131$07.00/0

shape, becomes unstable. The interfacial instability could be induced by the presence of gradients of pressure, temperature, concentration, etc., between bulk and interface and it could be described as a bulk-driven instability. Then, the interface grows against the efforts of a restoring force, such as surface tension. The linear regime is described by the usual Mullins–Sekerka[11] and Saffman–Taylor[12] instabilities. After the linear regime, structures like fingers or dendrites are generated. In general, these types of instabilities are highly nonlinear and nonlocal and are described by macroscopic models which contain the nonlinear effects by means of boundary conditions.

Driven diffusive systems (DDS)[13-17] are useful prototype models to study nonequilibrium interfacial instabilities and pattern formation.[18-24] In these models an external field is responsible for the instabilities and the nonequilibrium evolution to a final state is associated with the use of open boundary conditions. In Refs. 20 and 23, starting from a macroscopic model, two different types of linear instabilities have been studied. The first[20] is the Mullins–Sekerka-type instability. In DDS, the imbalance of fluxes responsible for the instability is generated by the external field. The second[23] is the so-called surface-driven instability. In contrast to the Mullins–Sekerka instability, which is bulk driven, the surface-driven instability is localized to the vicinity of the interface between the two coexisting phases and depends essentially on the orientation of the external field with respect to these phases.

An interesting aspect of the driven diffusive systems is that they could be described at a mesoscopic level by means of a relatively simple field model. This is a conserved time-dependent Ginzburg–Landau-like model, which contains a new flux term that takes into account the presence of the external field. In this sense, this model is a generalization of model B of critical[25] and phase separation[26] dynamics. In order to describe the evolution to a nonequilibrium state, open boundary conditions are used. In this paper we study the evolution of patterns from the short-time regime to the final state and the dependence of pattern formation on the boundary conditions. In Section 2, we present the model. In Section 3, we discuss the results of our numerical integrations. We use different types of open boundary conditions, such as periodic, antiperiodic, and fixed. For periodic boundary conditions, the two interfaces associated with a strip perpendicular to the external field become unstable. A characteristic concentration profile is generated with a kink–antikink structure in the direction of the external field. We also study these two interfaces separately by considering an isolated interface in the presence of antiperiodic and fixed boundary conditions. In this way, we reproduce the kink and antikink concentration profile of each interface, respectively. Then, from our numerical results,

we determine the linear dispersion relation associated with each interface. During the intermediate regime, we observe the growth of fingers. In particular, fingers with a highly characteristic shape are formed at the unstable interfaces with a kink concentration profile. Depending on the boundary conditions, the final state corresponds to strips (periodic boundary conditions), multifinger states, or a one-finger state (antiperiodic and fixed boundary conditions). In Section 3, we present an analytical analysis. We discuss the results for the initial growth of the different interfaces in terms of surface-driven[23] and Mullins–Sekerka[20] instabilities. The linear evolution of interfaces with kink concentration profile could be explained in terms of a surface-driven instability. Furthermore, the presence of antikink concentration profiles gives rise to a bulk instability of the Mullins–Sekerka type. For the long-time limit, we concentrate on the characterization of the one-finger state with triangular shape. We relate the tip width with the length introduced by the external field. A summary of conclusions is presented in Section 4.

2. THE FIELD MODEL

The model is described by the following equation for the concentration variable:

$$\frac{\partial \bar{c}}{\partial \tau} = \nabla^2 \frac{\delta \mathscr{H}}{\delta \bar{c}} - \nabla \cdot (\mathbf{E}' \sigma(\bar{c})) \tag{2.1}$$

where $\mathscr{H}$ is the Ginzburg–Landau free energy:

$$\mathscr{H} = \int \mathbf{dr} \left(-\frac{r}{2} \bar{c}^2 + \frac{u}{4} \bar{c}^4 + \frac{\xi_0^2}{2} |\nabla \bar{c}|^2 \right) \tag{2.2}$$

For a zero value of the external field $\mathbf{E}'$, we have the usual time-dependent Ginzburg–Landau equation for a conserved order parameter. The second term of the right-hand side of Eq. (2.1) contains the contribution to the total flux induced by $\mathbf{E}'$ acting on charged particles and $\sigma(\bar{c}) = 1 - a\bar{c}^2$ is the conductivity. For simplicity, in Eq. (2.1) we take a symmetric coupling between the conductivity and the concentration values. This coupling takes into account the decrease in the flux induced by $\mathbf{E}'$ by reducing temperature. The parameter a depends on temperature, and $a = 1$ for $T = 0$ and decreases by increasing T.

Equations (2.1)–(2.2) can be written in dimensionless form by

$$\frac{\partial c}{\partial t} = \nabla^2(-c + c^3 - \nabla^2 c) + \nabla \cdot (\mathbf{E} c^2) \tag{2.3}$$

where there is now only one parameter **E**. We consider **E** in the direction of the positive y coordinate. A stationary solution of Eq. (2.3) for a flat interface in two dimensions, with a nonzero constant flux $\mathbf{J} = J\hat{\mathbf{y}}$ imposed at the boundaries, is given by[20]

$$c_{\pm}(y) = \pm c_{\pm} \tanh\left(\frac{y}{\xi_{\pm}\sqrt{2}}\right) \tag{2.4}$$

where $c_{\pm}$ and $\xi_{\pm}$ are

$$c_{\pm} = \left(1 \pm \frac{\sqrt{2}}{2} E\right)^{1/2} \tag{2.5}$$

$$\xi_{\pm} = \frac{1}{c_{\pm}} \tag{2.6}$$

$\mathbf{J}_{\pm} = (1 - ac_{\pm}^2)\mathbf{E}'$ are the fluxes at the boundaries and $E = |\mathbf{E}|$. For zero **E**, Eq. (2.4) gives the standard kink solutions $c_{\pm}(y)|_{E=0} = \pm c_0(y)$, which describe the coexistence of two phases (rich and poor) with bulk concentration values $c_+ = c_- = c_0 = 1$ and interference width $\xi_+ = \xi_- = 1$ centered at $y = 0$. For a nonzero **E**, the two different solutions $c_+(y)$ and $c_-(y)$ have different bulk concentration values, Eq. (2.5), and interfacial widths, Eq. (2.6), depending on the orientation of **E** respect to the two phases.

3. NUMERICAL RESULTS

We have considered a discretization of Eq. (2.3) in a $W \times L$, rectangular lattice of different sizes. W is the size of the lattice in the x direction. **E** points to the positive y direction. We have used the Euler method with a mesh size $\Delta x = [1.0, 1.5]$ and time interval $\Delta\tau = [0.01, 0.2]$.

First, we consider periodic boundary conditions in both directions and we start with a strip perpendicular to the external field. As initial perturbation of the flat interfaces, we introduce a superposition of modes with random weights. In Fig. 1 we present a typical interfacial evolution for this case. Positive and negative values of the concentration correspond to black and white regions, respectively. The two interfaces of the strip are unstable and they develop structures during the process. For intermediate times, (Figs. 1b and 1c), fingers are formed and grow. In particular, we obtain a very characteristic triangular shape of the fingers for one of the interfaces. In the long-time regime, we obtain a pattern with two strips parallel to **E** (Fig. 1d). One expects, based on energetic reasons, that the final pattern would correspond to only one strip. However, this appears to be a very slow process in the absence of fluctuations.

In Fig. 2, we present the shape of the concentration profile developed in the initial stage of the temporal evolution described by Fig. 1. The matching of two kinks with different bulk concentration values gives as a result a kink–antikink profile. The kink could essentially be described by the $c_-(y)$ solution of Eqs. (2.4)–(2.6). Furthermore, the antikink profile presents a maximum concentration value slightly smaller than c_+ which rapidly decreases to c_-.

In the following, we treat the two interfaces of Fig. 1 separately. In this way, two different aspects could be studied. First, we are able to obtain numerically the dispersion relation characterizing the initial evolution of each interface separately and to compare them with the available theories.[20,23] Second, we obtain different behaviors of the interfaces in the

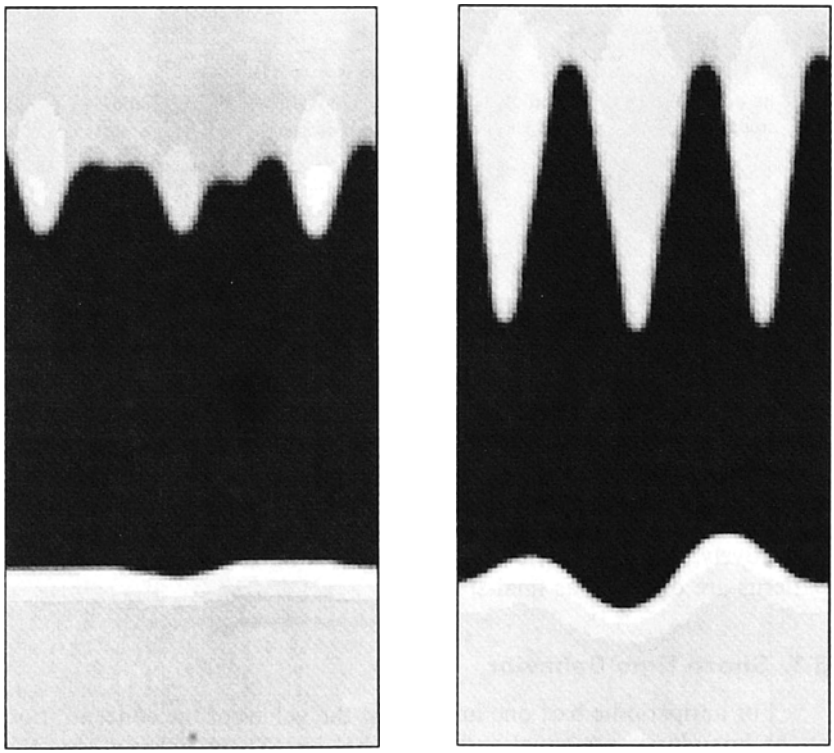

Fig. 1. Temporal evolution of interfaces with periodic b.c. and $W=75$, $L=150$, $E=0.3$. (a) $t=500$; (b) $t=2000$; (c) $t=4000$; (d) $t=20{,}000$.

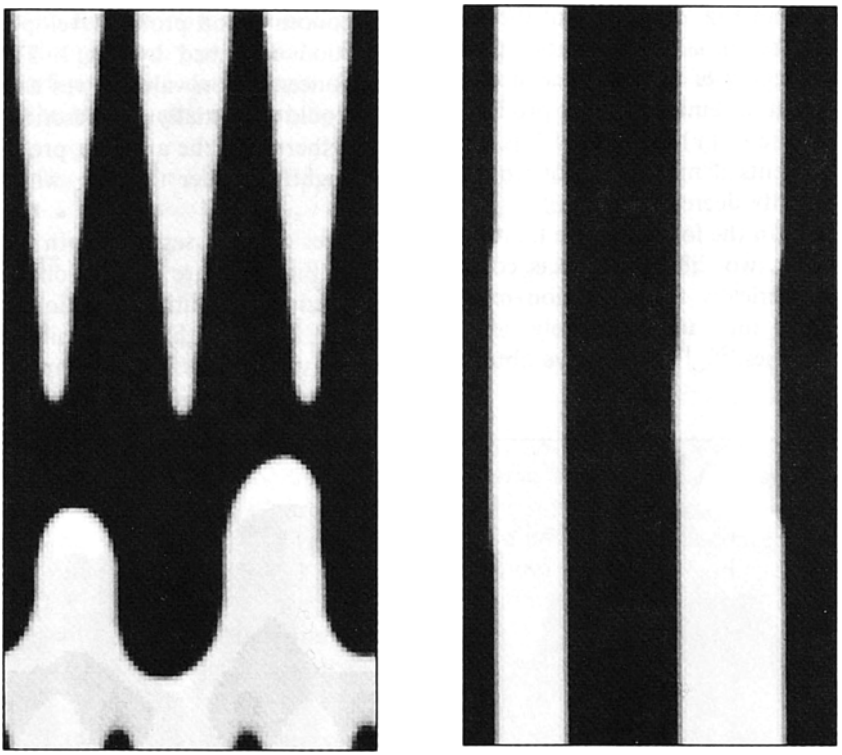

(c) (d)

Fig. 1 (*continued*)

long-time regime due to the use of different types of boundary conditions. For each isolated interface, we reproduce the concentration profile of Fig. 2. The kink and antikink profiles in the right and left side of Fig. 2 are obtained by considering antiperiodic and fixed boundary conditions, respectively. For these boundary conditions multifinger and also one-finger patterns are obtained as final states.

3.1. Short-Time Behavior

For antiperiodic b.c., one imposes that the values of the concentration at the boundaries are equal and of opposite sign. Then, starting from the kink solution profile corresponding to $E=0$, the concentration values, which depend on the external field, readjust rapidly to the kink profile given by Eq. (2.4) with $E\neq 0$. In this case, we observe that the interface is either unstable or stable depending on the orientation of the external field

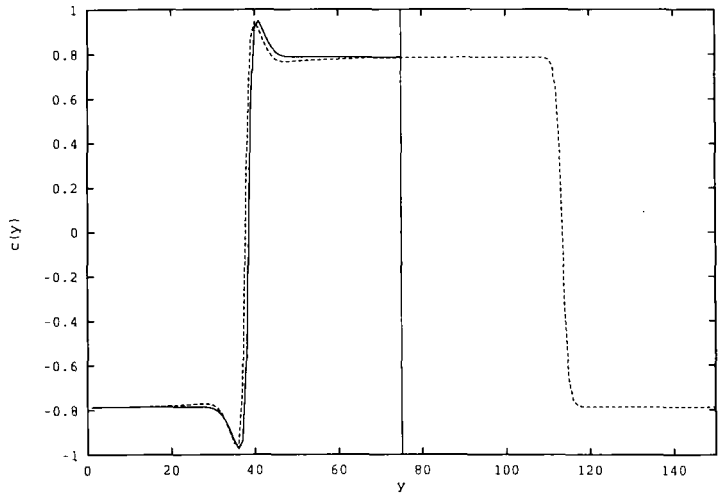

Fig. 2. Initial concentration profiles. Dotted line: periodic b.c. Continuous line on the left side of the central vertical line: fixed b.c. **E** points to the positive y direction.

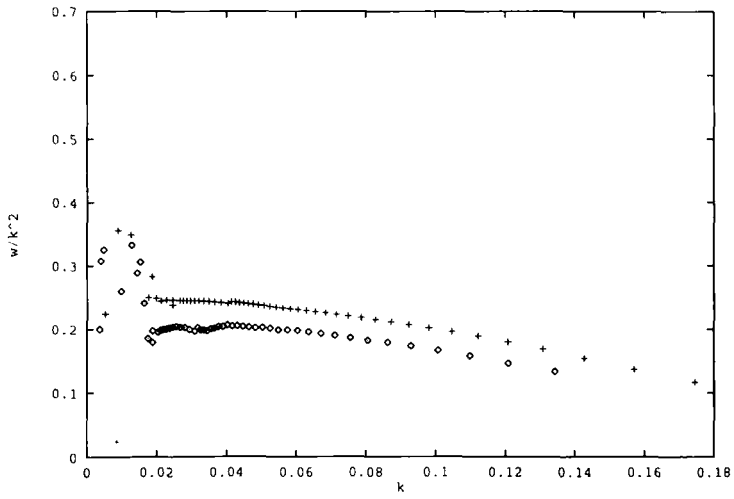

Fig. 3. Numerical results of Eq. (2.3) for the linear dispersion relation. +: antiperiodic b.c. ◇: fixed b.c.

with respect to the two coexisting phases.[23] In particular, $c_+(y)$ and $c_-(y)$ are stable and unstable, respectively. For an unstable interface, the external field points from the rich (black) to the poor (white) phases, as in the case of the kink profile in Fig. 2 (that is, the interface at the top of Fig. 1).

For fixed boundary conditions, the values of the concentration at the boundaries are fixed. In this case, depending on whether the concentration at the boundary is smaller or larger than the maximum concentration value, the interface is unstable or stable,[20] respectively. Following this argument, the antikink profile in Fig. 2 is unstable (that is, the interface at the bottom of Fig. 1).[2]

To give a quantitative characterization of the initial temporal evolution, we present the numerical results obtained for the linear dispersion for both antiperiodic and fixed boundary conditions in Fig. 3. For a small perturbation of the planar interface, $y(t) = A \exp(w(k) \cdot t)$, we obtain in both cases that $w(k) \approx k^2$ in the region of small k. For very small values of k, numerical errors are more important due to the very small values of $w(k)$. In the following section we give a theoretical interpretation of the results presented.

3.2. Long-Time Behavior

We have performed numerical integrations in the long-time regime for the unstable isolated interface in the presence of antiperiodic (Figs. 4a and 4b) and fixed (Fig. 4c) boundary conditions. The characteristic triangular-shaped fingers observed in Fig. 1 for periodic boundary conditions are also developed during the intermediate temporal regime for antiperiodic boundary conditions. In this case, we observe a very rapid competition between fingers. For lattices in which the rate L/W is not large, a multifinger state is obtained, as in Fig. 4a. For large L/W, the competition between fingers proceeds until only one finger is left, as in Fig. 4b. In Figs. 5a and 5b we present the evolution of only one finger with two different tip widths. We find that the final tip width is independent of the initial width and appears to depend only on the value of the external field.

For fixed boundary conditions, the unstable interface also develops fingers, but in this case they have not a triangular shape, but the ones that

[2] For the interface with the antikink profile, in the initial stages a relaxation of the initial perturbations is obtained.[23] However, after this transient the interface becomes unstable with a perturbation of smaller wavevector k.

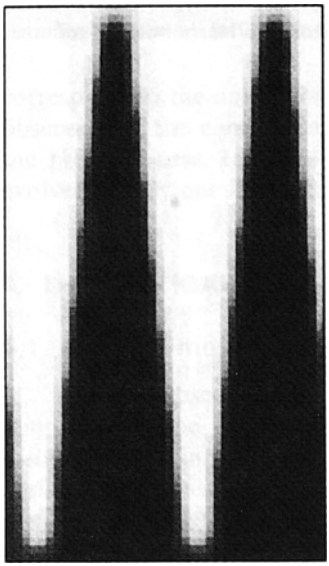

(a)

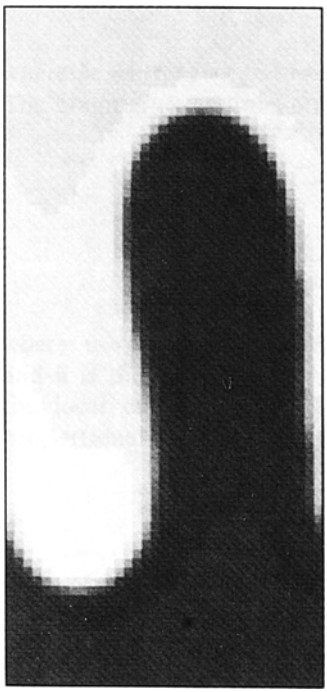

(c)

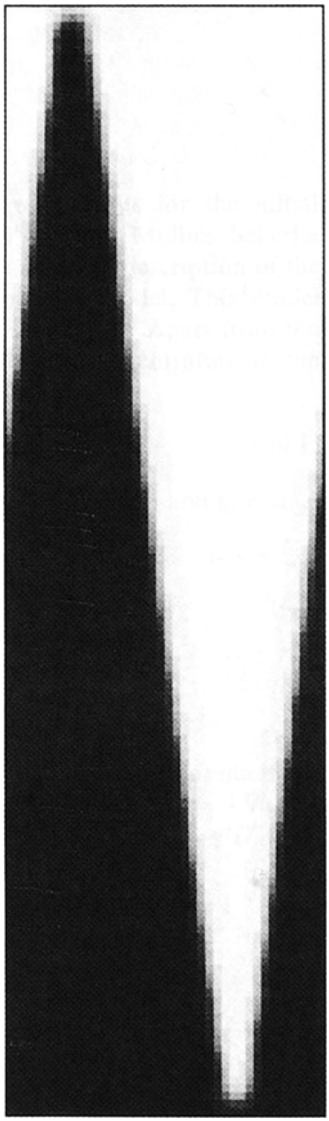

(b)

Fig. 4. Long-time evolution of interfaces with (a) multifinger state with antiperiodic b.c., $W = 40$, $L = 70$, $E = 0.5$, and $t = 10{,}000$. (b) One-finger state with antiperiodic boundary conditions, $W = 40$, $L = 140$, $E = 0.5$, and $t = 10{,}000$. (c) One-finger state with fixed b.c., $W = 35$, $L = 75$, $E = 0.3$, and $t = 1500$.

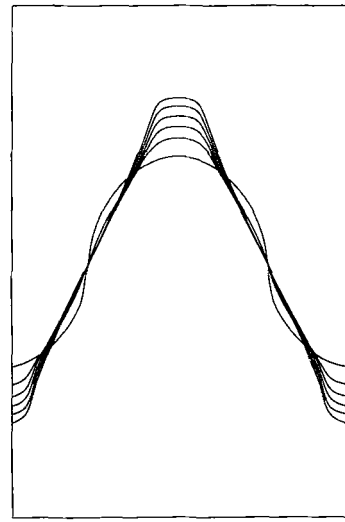

(a)

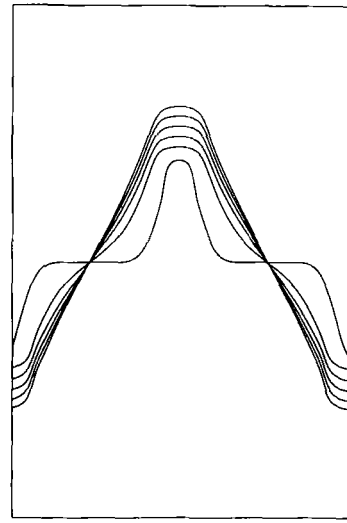

(b)

Fig. 5. One-finger state with antiperiodic b.c. and different initial tip width λ for $E=0.3$ (a) $\lambda > \lambda_{tip}$. (b) $\lambda < \lambda_{tip}$. In both cases the final tip width is λ_{tip}.

correspond to the antikink concentration profile in Fig. 1. In this case, we observe that the competition between fingers is very slow compared with the previous case. In Fig. 4c we present a pattern in which the interface evolves to only one finger. In this case, E points to the negative y direction.

4. THEORETICAL ANALYSIS

4.1. Short-Time Behavior

In this subsection we explain the numerical results for the initial temporal regime in terms of surface-driven[23] and Mullins–Sekerka instabilities.[20] In ref. 23 we have presented an analytical description of the surface-driven instability in terms of a macroscopic model. This model could be derived from the mesoscopic model, Eq. (2.3).[24] Apart from the dynamic equation for the temporal evolution of the concentration in the bulk

$$\partial_t \delta c = -\nabla \cdot \mathbf{j}_{\pm} = D\nabla^2 \delta c \pm Q\mathbf{E} \cdot \nabla \delta c \tag{4.1}$$

where $\delta c = c(\mathbf{r}, t) - c_{\pm}$, the diffusion coefficient $D = 3c_{\pm}^2 - 1$, and $Q = 2c_{\pm}$. The boundary equations are

$$\delta c|_I = \Gamma \mathscr{K} \pm \frac{\beta}{4} \mathbf{E} \cdot (\hat{\mathbf{u}} - \hat{\mathbf{y}}) \tag{4.2}$$

$$v = \frac{1}{\Delta c} [(\mathbf{j}_+ - \mathbf{j}_-) \cdot \hat{\mathbf{u}}]_I + \frac{\beta}{\Delta c} \mathscr{K} \mathbf{E} \cdot \hat{\mathbf{u}} \tag{4.3}$$

where $\mathbf{u} = u\hat{\mathbf{u}}$, is the normal coordinate with respect to the interface, and $\hat{\mathbf{u}}$ is the unitary vector that points to the rich phase, $\mathscr{K} = -\nabla \cdot \hat{\mathbf{u}}$ is the local curvature, $\Delta c = 2c_{\pm}$ is the concentration gap, $\Gamma = \gamma / D\,\Delta c$ is proportional to the surface tension

$$\gamma = \int_{-\infty}^{\infty} du \left(\frac{dc_0(u)}{du} \right)^2 = \frac{2\sqrt{2}}{3}$$

and

$$\beta = \int_{-\infty}^{\infty} du [\sigma(c_0(u)) - \sigma(c_0)] = 2\sqrt{2}$$

The subscript I means the limiting values as the interface is approached from the bulk phases.

The second term of the right-hand side of Eq. (4.1) contains the flux term induced by the external field. Equation (4.2) is the Gibbs–Thomson relation, and is also affected by the presence of $\mathbf{E}$. The new term accounts for the correction of the concentration values in $c(u)$, $c_{\pm}$ of Eqs. (2.4) and (2.5) because the interface is locally tilted with respect to the field direction. However, in the linear approximation, the contribution of this term is negligible for $|\mathbf{E}\cdot\hat{\mathbf{u}}|\approx E$. The most important contribution regarding the destabilization effects is given by the new contribution, the second term of the right-hand side, of the continuity equation (4.3). This new term contains the contribution of a flux along the interface by the external field. It arises from the variation of the tangential current, which depends on the orientation of the interface with respect to the external field. In this sense, we talk about a surface-driven instability and the results do not depend on the type of boundary conditions. The sign of this contribution depends only on the product $\mathbf{E}\cdot\hat{\mathbf{u}}$. For example, it gives a destabilizing contribution to interfaces with the same orientation as that on the right side of Fig. 2 and a stabilizing contribution for the opposite direction. These results are in agreement with our numerical results for the isolated interface with antiperiodic boundary conditions. For large values of $\mathbf{E}$, this term dominates, the interface decouples from the bulk, and we can talk about a local model.

The linear dispersion relation for a small perturbation of the planar interface can be obtained from Eqs. (4.1)–(4.3),[23]

$$w(k)=-\frac{\Gamma k^2}{\Delta c}\{-EQ+[(EQ)^2+(2Dk)^2]^{1/2}\}+\frac{\alpha Ek^2}{\Delta c} \tag{4.4}$$

where $\alpha=\beta-2Q\Gamma$.

The destabilizing effect in Eq. (4.4) comes from the last term. From Eq. (4.4) we find that the small-k limit gives a $w(k)\approx k^2$ behavior in accordance with the numerical results for the dispersion relation of Fig. 3.

Furthermore, the Mullins–Sekerka-type instability of ref. 20 could explain the results for the antikink-profile interfaces of Fig. 1 or, equivalently, for the result obtained for fixed boundary conditions. In this case, the characteristic ramp profile responsible for the instability is induced by the external field. Apart from the bulk equation, Eq. (4.1), we have the corresponding boundary equation together with Eq. (4.3).

$$\delta c|_I=\Gamma\mathscr{K}\pm\frac{\beta}{4}\mathbf{E}\cdot(\hat{\mathbf{u}}-\hat{\mathbf{y}})-\frac{\mathbf{J}_0}{D}\cdot\mathbf{y} \tag{4.5}$$

where $\mathbf{J}_0(\mathbf{E})/D$ accounts for the slope of the ramp. The term proportional to $\mathbf{E}$ is associated with the surface-driven instability and gives a stabilizing

contribution due to the orientation of the field with respect to the antikink interface of Fig. 1.

From these equations, the dispersion relation is

$$w(k) = \left(\frac{J_0}{2D\,\Delta c} - \frac{\Gamma k^2}{\Delta c}\right)\{+EQ + [(EQ)^2 + (2Dk)^2]^{1/2}\} - \frac{\alpha E k^2}{\Delta c} \tag{4.6}$$

In this case, the destabilizing term is the one proportional to J_0. We also obtain a k^2 behavior in the small-k limit in agreement with the results of the numerical integration (Fig. 3). For very small values of E, the ramp profile is also very small and only very larger wavelength modes are unstable (see preceding footnote).

4.2. Long-Time Regime

In this subsection we present theoretical arguments in order to characterize the shape of the triangular finger at the long-time limit. One of the essential ingredients of this analysis is related to the tip width of the fingers. As we conclude from Fig.5, the tip width depends on the value of E and different initial widths evolve to the same final one. Furthermore, we obtain a smaller tip width by increasing E. Apart from L and W, there is another length introduced by the external field E. The external field has dimensions of the inverse of a length. The size of the tip of the finger is simple related to this length. In fact, we observe that the tip width in the long-time regime is not very different from that of the fingers in the linear regime. Then, following this argument, the tip width of the fingers can be calculated approximately from the linear dispersion relation. In this way, the tip width at initial stages is

$$\lambda_{\max} = \frac{2\pi}{k_{\max}} \tag{4.7}$$

where $k_{\max}$ is the fastest mode of the dispersion relation calculated from Eq. (4.4). In particular, we find that $k_{\max} \propto E$. For larger E we obtain a shift to larger values of $k_{\max}$ and then smaller tips for the fingers, in accordance with the numerical simulations. Therefore, the initial number of fingers N is

$$N \sim \frac{W}{\lambda_{\max}} \tag{4.8}$$

At long times, the tip width λ_{tip} is approximately $\lambda_{\text{tip}} \sim \lambda_{\max}$. In Fig. 6 we present the results for $\lambda_{\max}$, determined from Eq. (4.4), and λ_{tip} versus E.

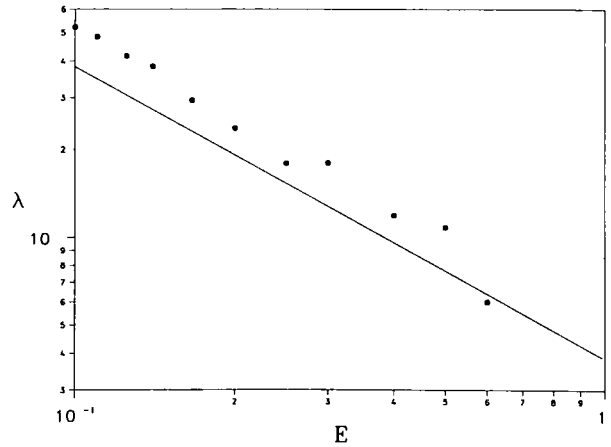

Fig. 6. Comparison between λ_{tip} and λ_{max} versus E. The continuous line has been obtained by calculating the maximum of $w(k)$ from Eq. (4.4). The dots are the numerical results for λ_{tip} calculated as explained in the text.

To calculate λ_{tip} we have used the long-time patterns obtained from our numerical simulations and we have considered that the tip ends at the points where the second derivative of the interfacial curve is zero. We obtain that our prediction about the dependence of $\lambda_{tip} \propto 1/E$ is essentially correct, but there is a constant positive shift between the values of λ_{max} and λ_{tip}. This could be associated in part with the criterion chosen to determine λ_{tip}, which overestimates the tip width. Furthermore, it could also be attributed in part to the highly nonlinear effects present in the long-time limit that do not affect λ_{max}.

Furthermore, we observe that the angle θ between the lateral finger interface and the x direction is not fixed, but depends on the tip width and on the number of fingers at each time. For large values of L/W and in the long-time limit for which only one finger remains after the disappearance of all the rest, the shape of the one finger could be determined in terms of L, W, and λ_{tip} by the following expression:

$$\theta = \arctan\left(\frac{2L - \lambda_{tip}}{W - \lambda_{tip}}\right) \tag{4.9}$$

5. SUMMARY

We have studied numerically the short- and long-time regime of the evolution of interfaces in driven diffusive systems with periodic, antiperiodic, and fixed boundary conditions. For periodic boundary condi-

tions, we observe that both interfaces of an initial strip perpendicular to the external field become unstable. During the intermediate temporal regime, fingers are developed. In particular, fingers with a triangular shape are developed for one of the interfaces. Different interfacial instability mechanisms are associated with each interface. We have studied numerically the linear dispersion relation of both interfaces by considering each one independently, in the presence of antiperiodic and fixed boundary conditions. A theoretically predicted surface-driven instability seems to be the responsible for the instability giving rise to triangular-shaped fingers. The other interface has a characteristic ramp profile and the instability could be explained in terms of a Mullins–Sekerka-type mechanism. For the long-time regime we obtain strips in the periodic boundary condition case. For antiperiodic and fixed boundary conditions the multifinger state and one-finger state could be obtained. For antiperiodic boundary conditions we have studied the long-time evolution of only one triangular finger. We give an explanation of the triangular shape in terms of the length associated with the external field.

ACKNOWLEDGMENTS

We are grateful to D. Jasnow and C. Yeung for useful discussions. We thank the Dirección de Investigación Científica y Técnica (Spain) under Pro. No. PB90-0030 for support. We also acknowledge the support of CESCA (Centre de Supercomputació de Catalunya), where the numerical computations were performed.

REFERENCES

1. J. S. Langer, in *Proceedings of Les Houches Summer School: Chance and Matter*, J. Souletie *et al.*, eds. (Elsevier, 1987).
2. D. A. Kessler, J. Koplik, and H. Levine, *Adv. Phys.* **35**:255 (1988).
3. P. Pelce, in *Dynamics of Curved Fronts* (Academic Press, New York, 1988).
4. D. Bensimon, L. P. Kadanoff, S. Liang, B. I. Schraiman, and Ch. Tang, *Rev. Mod. Phys.* **58**:977 (1986).
5. D. Jasnow, in *Far from Equilibrium Phase Transitions* (Springer-Verlag, Berlin, 1988).
6. G. Tryggvason and H. Aref. *J. Fluid Mech.* **136**:1 (1983).
7. J. V. Maher, *Phys. Rev. Lett.* **54**:1498 (1985).
8. D. A. Kessler and H. Levine, *Phys. Rev. A* **33**:3625 (1986).
9. D. Jasnow and J. Vinals, *Phys. Rev. A* **40**:3864 (1989).
10. J. Casademunt and D. Jasnow, *Phys. Rev. Lett.* **67**:3677 (1991): J. Casademunt, D. Jasnow, and A. Hernández-Machado, *Int. J. Mod. Phys. B* **6**:1647 (1992).
11. W. W. Mullins and R. F. Sekerka, *J. Appl. Phys.* **35**:444 (1964).
12. P. G. Saffman and G. I. Taylor, *Proc. R. Soc. A* **245**:312 (1958).
13. S. Katz, J. L. Lebowitz, and H. Spohn, *Phys. Rev. B* **28**:1655 (1983); *J. Stat. Phys.* **34**:497 (1984).

14. K.-T. Leung and J. L. Cardy, *J. Stat. Phys.* **44**:567 (1986); H. K. Janssen and B. Schimttman, *Z. Phys. B* **64**:503 (1986).
15. J. L. Vallés and J. Marro, *J. Stat. Phys.* **43**:441 (1986).
16. R. Dickman, *Phys. Rev. A* **38**:2588 (1988).
17. K.-T. Leung, B. Schmittmann, and R. K. P. Zia, *Phys. Rev. Lett.* **62**:1772 (1989).
18. A. Hernández-Machado and D. Jasnow, *Phys. Rev. A* **37**:656 (1988); A. Hernández-Machado, H. Guo, J. L. Mozos, and D. Jasnow, *Phys. Rev. A* **39**:4783 (1989).
19. K.-T. Leung, *J. Stat. Phys.* **50**:405 (1988).
20. K.-T. Leung, *J. Stat. Phys.* **61**:345 (1990).
21. D. H. Boal, B. Schmittmann, and R. K. P. Zia, *Phys. Rev. A* **43**:5214 (1991).
22. C. Yeung, T. Rogers, A. Hernández-Machado, and D. Jasnow, *J. Stat. Phys.* **66**:1071 (1992).
23. C. Yeung, J. L. Mozos, A. Hernández-Machado, and D. Jasnow, *J. Stat. Phys.* **70**:1149 (1993).
24. J. L. Mozos, Ph.D. thesis, Universitat de Barcelona (1993).
25. P. C. Hohenberg and B. I. Halperin, *Rev. Mod. Phys.* **49**:435 (1977).
26. J. D. Gunton, M. San Miguel, and P. S. Shani, in *Phase Transitions and Critical Phenomena*, Vol. 8, C. Domb and J. L. Lebowitz, eds. (Academic Press, New York, 1983), p. 267.